

# Shell model of superfluid turbulence

D. H. Wacks\* and C. F. Barenghi

*School of Mathematics and Statistics, University of Newcastle,*

*Newcastle upon Tyne, NE1 7RU, UK*

## Abstract

Superfluid helium consists of two inter-penetrating fluids, a viscous normal fluid and an inviscid superfluid, coupled by a mutual friction. We develop a two-fluid shell model to study superfluid turbulence. We investigate the energy spectra and the balance of fluxes between the two fluids as a function of temperature in continuously forced turbulence, and, in the absence of forcing, the decay of turbulence. We furthermore investigate deviations from the  $k^{-5/3}$  spectrum caused by the mutual friction force. We compare our results with experiments and existing calculations. We find that, at sufficiently low temperatures a build-up of energy develops at high wavenumbers suggesting the need for a further dissipative effect, such as the Kelvin wave cascade and phonon emission.

PACS numbers: 67.25.dk Vortices and turbulence in superfluid  $^4\text{He}$

47.32.C- Vortex dynamics

47.27.Gs Homogeneous isotropic turbulence

---

\* d.h.wacks@ncl.ac.uk

## I. INTRODUCTION

Helium II (the low temperature, quantum phase of liquid  ${}^4\text{He}$ ) consists of two interpenetrating fluid components [1]: the inviscid superfluid (associated with the quantum ground state) and the viscous normal fluid (consisting of thermal excitations). Each fluid component has its own density and velocity field,  $\rho^s, \mathbf{u}^s$  for the superfluid and  $\rho^n, \mathbf{u}^n$  for the normal fluid, where  $\rho = \rho^s + \rho^n$  is helium's density and the relative proportion of superfluid and normal fluid depends on the absolute temperature  $T$ .

What makes helium II particularly interesting is that the superfluid vorticity is concentrated in thin, discrete vortex filaments of fixed (quantized) circulation  $\kappa = h/m = 9.97 \times 10^{-4} \text{ cm}^2/\text{s}$ , where  $h$  is Planck's constant and  $m$  the mass of one  ${}^4\text{He}$  atom. The vortex filaments interact with the thermal excitations, causing a mutual friction between superfluid and normal fluid [2].

Turbulence in helium II (quantum turbulence) is easily generated in the laboratory by stirring or pushing liquid helium with grids and propellers [3–5], vibrating forks [6] or other means. Quantum turbulence is a complex state [7] in which normal fluid eddies of arbitrary shapes and strengths interact with a tangle of discrete vortex filaments of fixed strength. Despite the two-fluids nature of quantum turbulence, experiments have shown remarkable similarities with turbulence in ordinary fluids (classical turbulence), for example the same pressure drops along pipes and channels [8], drag crisis behind a sphere [9], and Kolmogorov energy spectrum [10]. The last property, which is our particular concern in this paper, describes how the energy of the flow is distributed over the length scales in homogeneous isotropic turbulence.

Whereas turbulence in ordinary fluids is studied on the firm ground of the Navier-Stokes equation, there is not such an established equation for turbulent helium II. Existing numerical simulations [11, 12] of quantum turbulence follow the approach of Schwarz [13], who calculated the properties of the vortex tangle by integrating in time the motion of a great number of individual vortex filaments in the presence of a prescribed normal fluid, neglecting the back reaction of the superfluid onto the normal fluid.

The aim of this work is to gain insight into self-consistent turbulent two-fluids hydrodynamics using a shell model [14]. In classical fluid dynamics [15] shell models are idealized truncated models of the Navier-Stokes equation which neglect any geometry of the flow but

describe the Richardson cascade, its properties (e.g. the Kolmogorov energy spectrum) over a wide range of scales and times. In the less understood context of helium II, shell models allow us to explore the interaction of normal fluid and superfluid in the inertial and dissipative ranges in a relatively simple way. What happens at very large length scales [16] where finite-size effects may affect the dynamics of the energy-containing eddies is beyond the scope of this work.

## II. MODEL

### A. Classical GOY model

The classical Navier-Stokes equation is

$$\rho\left(\frac{\partial \mathbf{u}}{\partial t} + \mathbf{u} \cdot \nabla \mathbf{u}\right) = -\nabla p + \mu \nabla^2 \mathbf{u}, \quad (1)$$

with the incompressibility condition  $\nabla \cdot \mathbf{u} = 0$ , where  $\mathbf{u}$  is the velocity,  $p$  the pressure,  $\rho$  the density and  $\mu$  the viscosity. Starting from the works of Gledzer [17] and Yamada & Okhitani [18], a variety of shell models have been developed [19] to study turbulent solutions of Eq. 1. The GOY model, named after the pioneering authors, is a finite-dimensional dynamical system which describes the dynamics of idealised (complex) Fourier components of the velocity field,  $u_m$  corresponding to wavenumber  $k_m$ ; the index  $m$  ( $m = 1, \dots, M$ ) is called the shell index. The wavenumbers are geometrically distributed in k-space,  $k_m = k_0 \lambda^m$ , where  $k_0$  is a reference wavenumber and  $\lambda > 1$ . The equations of motion are

$$\left(\frac{d}{dt} + \nu k_m^2\right) u_m = G_m[u] + f \delta_{m,m'}, \quad (2)$$

for  $m = 1, \dots, M$ , where  $\nu = \mu/\rho$  is the kinematic viscosity,  $\delta_{m,m'}$  is Kronecker's delta, and  $f$  is the amplitude of external forcing applied on a particular shell  $m = m'$ . The inertial term  $G_m[u]$  is quadratically nonlinear and local in k-space, coupling  $u_m$  with its nearest neighboring shells; more precisely we have

$$G_m[u] = i(c_m^{(1)} \bar{u}_{m+1} \bar{u}_{m+2} + c_m^{(2)} \bar{u}_{m-1} \bar{u}_{m+1} + c_m^{(3)} \bar{u}_{m-1} \bar{u}_{m-2}), \quad (3)$$

where  $\bar{u}$  denotes the complex conjugate of  $u$ , and

$$c_m^{(1)} = a k_m, \quad c_m^{(2)} = b k_{m-1}, \quad c_m^{(3)} = c k_{m-2}, \quad (4)$$

The boundary conditions are  $u_m = 0$  for  $m \leq 0$ ,  $m > M$  and

$$c_1^{(2)} = c_1^{(3)} = c_2^{(3)} = c_{M-1}^{(1)} = c_M^{(1)} = c_M^{(2)} = 0, \quad (5)$$

The coefficients  $a = 1$ ,  $b = -1/2$ ,  $c = -1/2$  and  $\lambda = 2$  are chosen so that in the steady ( $d/dt = 0$ ), unforced ( $f = 0$ ), inviscid ( $\nu = 0$ ) case the nonlinear interaction conserves the two quadratic invariants of the 3-dimensional Euler equation, energy and helicity,

$$E = \frac{1}{V} \int \frac{1}{2} \mathbf{u} \cdot \mathbf{u} dV, \quad H = \frac{1}{V} \int \boldsymbol{\omega} \cdot \mathbf{u} dV, \quad (6)$$

(where  $\boldsymbol{\omega} = \nabla \times \mathbf{u}$  and  $V$  is volume) which are identified as

$$E = \frac{1}{2} \sum_{m=1}^M |u_m|^2 = \sum_{m=1}^M E_m k_m, \quad (7)$$

where

$$E_m = \frac{|u_m|^2}{2k_m}, \quad (8)$$

is the spectral energy associated with shell  $m$ , and

$$H = \frac{1}{2} \sum_{m=1}^M (-1)^m \lambda^m |u_m|^2. \quad (9)$$

## B. Two-fluids equations

The two-fluids equations of helium II are [1]

$$\rho^s \left( \frac{\partial \mathbf{u}^s}{\partial t} + \mathbf{u}^s \cdot \nabla \mathbf{u}^s \right) = -\frac{\rho^s}{\rho} \nabla p + \rho^s S \nabla T - \mathbf{F} \quad (10)$$

$$\rho^n \left( \frac{\partial \mathbf{u}^n}{\partial t} + \mathbf{u}^n \cdot \nabla \mathbf{u}^n \right) = -\frac{\rho^n}{\rho} \nabla p - \rho^s S \nabla T + \mu \nabla^2 \mathbf{u}^n + \mathbf{F} \quad (11)$$

with  $\nabla \cdot \mathbf{u}^s = \nabla \cdot \mathbf{u}^n = 0$ , where  $S$  is the specific entropy. Hereafter we denote by  $\nu^n = \mu/\rho^n$  the kinematic viscosity of helium II. If  $\mathbf{F} = 0$  and  $\nabla \times \mathbf{u}^s = \boldsymbol{\omega}^s = 0$ , Eqs. 10 and 11 reduce to Landau's two-fluids equations, which describe the well-known mechanical and thermal behaviour of helium II in the absence of vortex lines. In the presence of vortices, the mutual friction  $\mathbf{F}$  which couples the two fluids depends on the vortex line density  $L$

(vortex length per unit volume), or, more precisely, on some suitably defined coarse-grained vorticity field  $\boldsymbol{\omega}^s$ . Unfortunately the form of  $\mathbf{F}$  is uncertain. The form given by Hall & Vinen [20] accounts for experiments in rotating cylinders and Taylor-Couette flow [21], in which vortices are either straight or curved, but still polarised in the same direction. In the case of turbulent flow, vortex filaments may be random or partially polarised, so the relation between the coarse-grained vorticity  $\boldsymbol{\omega}^s$  and the vortex line density  $L$  is not clear. Hereafter for the sake of simplicity, we assume the Gorter-Mellink [22] form

$$\mathbf{F} = \frac{B\rho^s\rho^n}{2\rho}\kappa L(\mathbf{u}^s - \mathbf{u}^n), \quad (12)$$

where  $B$  is a known temperature dependent mutual friction coefficient. This form for the mutual friction is motivated by dimensional arguments and is consistent with the method employed to measure vortex line density in experiments. It has been widely used in the quantum turbulence literature [2, 7, 23–26].

### C. Two-fluids GOY model

The natural generalization of Eq. 2 to two fluids is

$$\frac{d}{dt}u_m^s = G_m[u^s] - F_m + f^s\delta_{m,m'}, \quad (13)$$

$$\left(\frac{d}{dt} + \nu^n k_m^2\right)u_m^n = G_m[u^n] + \frac{\rho^s}{\rho^n}F_m + f^n\delta_{m,m'}, \quad (14)$$

where the nonlinear term for each fluid is as in Eq. 3, and the mutual friction is

$$F_m = \alpha\kappa L(u_m^s - u_m^n). \quad (15)$$

The temperature dependence of the friction coefficient  $\alpha = B\rho^n/(2\rho)$  is well-known [27]. For consistency, the vortex line density  $L$  is not an arbitrary parameter, but is identified as  $L = Q^{1/2}/\kappa$  where the superfluid enstrophy  $Q$  is

$$Q = \sum_{m=1}^M \frac{1}{2}k_m^2 |u_m^s|^2. \quad (16)$$

Clearly this model, which describes superfluid vorticity as a continuum, is meaningful only for length scales bigger than the average intervortex spacing  $\ell \approx L^{-1/2}$ , that is to say for wavenumbers  $k_m < k_\ell = 1/\ell = L^{1/2}$ .

In a recent paper, Roche *et al.* [23] solved equations similar to our Eqs. 10 and 11 in the presence of continuous forcing applied to the fluid with the greater density, thus performing the first Direct Numerical Simulations (DNS) of two-fluids hydrodynamics. Unlike our two-fluids shell model, their two-fluids DNS contained an artificial superfluid viscous force  $\nu^s \rho^s \nabla^2 \mathbf{u}^s$  at the right hand side of Eq. 10. The introduction of this unphysical term was motivated by numerical analysis. They set the ratio  $\nu^n/\nu^s = 4$  to minimize the effect of the artificial viscosity while preserving the stability of the calculation. We stress that our two-fluids shell model (see Eq. 13) does not need such an artificial term. Another related model is the large-eddy calculation of Merahi *et al.* [28]

### III. RESULTS

#### A. Forced Turbulence

Unless stated otherwise, the results which we present are obtained by numerically integrating in time Eqs. 13 and 14 for  $M = 18$ ,  $k_0 = 2^{-4}$ . The same forcing (typically  $f^s = f^n = (1 + i) \times 5 \times 10^{-3}$ ) is applied to shell  $m = 4$  for both superfluid and normal fluid. A typical initial condition is  $w_m^j = (1 + i)k_m \exp(-k_m^2/2)$ , ( $j = n, s$ ), for which  $E_m^j = k_m \exp(-k_m^2)$ . The time stepping combines the Crank-Nicolson method for the diffusion term and the Adams-Bashforth method for the other terms; the typical time step is  $\Delta t = 5 \times 10^{-6}$ . We stop the time integration after the spectrum saturates, making sure that the elapsed time is of the order of 10 large eddy turnover times (about 100 turnover times of the forcing wavenumber), which is typically of the order of 500 s. We find that, once saturation is achieved, time averaged spectra are the same as ensemble averaged spectra (obtained using randomly phase shifted realisations).

To study the temperature dependence of the results, we consider three temperatures  $T = 2.157$  K, 1.96 K and 1.44 K which hereafter we refer to as high, medium and low temperatures [23]. The values of  $\rho^s$ ,  $\rho^n$ ,  $\rho$ ,  $\nu$  and  $\alpha$  in TABLE 1. corresponding to these temperatures are The resulting normal fluid fractions,  $\rho^n/\rho^s$ , are approximately 10, 1 and 0.1 for high, medium and low temperatures respectively.

Fig. 1 (top) shows superfluid and normal fluid spectra at high temperature. It is apparent that superfluid and normal fluid velocity lock onto each other by the mutual friction

$T$ (K)	$\rho^s$ (g/cm <sup>3</sup> )	$\rho^n$ (g/cm <sup>3</sup> )	$\rho$ (g/cm <sup>3</sup> )	$\nu$ (cm <sup>2</sup> /s)	$\alpha$
2.157	0.01510	0.12939	0.14449	$1.526 \times 10^{-4}$	1.045
1.96	0.07335	0.07221	0.14556	$9.694 \times 10^{-5}$	0.245
1.44	0.13251	0.01264	0.14515	$9.538 \times 10^{-5}$	0.059

TABLE I. Helium parameters used in our calculations.

over many length scales as envisaged by Vinen and Niemela [7] and Barenghi *et al.* [29]. Furthermore a closer inspection of the complex  $u_m$  throughout the inertial subrange reveals that  $\Re(u_m^n) = \Re(u_m^s)$  and  $\Im(u_m^n) = \Im(u_m^s)$  to at least 4dp. Both spectra are consistent with the Kolmogorov scaling  $k^{-5/3}$  (denoted by the solid line) over a wide inertial range  $k_0 \ll k \ll k_\ell$ , as observed in experiments [10] and DNS of two-fluids hydrodynamics [23]. The vertical dotted line denotes the wavenumber  $k_\ell$  which corresponds to the intervortex spacing. To make the Kolmogorov scaling more evident, we plot the compensated spectra  $k^{5/3} E_k$  (see Fig. 1 (top,inset)). It is apparent that the superfluid spectrum extends to bigger wavenumbers than the normal fluid's: this is because there are no viscous forces acting on the superfluid; nevertheless, the superfluid spectrum decays at large  $k$  because superfluid motion is damped by mutual friction. We confirmed that the development of a  $k^{-5/3}$  spectrum is dependent neither on our choice of initial condition nor on the fact that we force both fluids.

It is instructive to consider the scale-by-scale energy budget per unit mass. Using Eqs. 13 and 14 and the fact that

$$\frac{dE_m}{dt} = \frac{1}{2} \left( \frac{du_m}{dt} \bar{u}_m + u_m \frac{d\bar{u}_m}{dt} \right)$$

we obtain

$$\frac{dE_m^n}{dt} = T_m^n + D_m^n + M_m^n + \epsilon_{inj}^n \delta_{m,4}, \quad (17)$$

$$\frac{dE_m^s}{dt} = T_m^s + M_m^s + \epsilon_{inj}^s \delta_{m,4}, \quad (18)$$

where

$$T_m^j = -\Im(G_m[u^j]u_m^j) \quad (19)$$

are the energy transfer rates arising from the triadic interactions between Fourier modes

within each fluid,

$$D_m^n = -2\nu^n k_m^2 E_m^n \quad (20)$$

is the rate of viscous dissipation in the normal fluid,

$$M_m^n = \frac{\rho^s}{\rho^n} \Re(F_m \bar{u}_m^n) \quad (21)$$

and

$$M_m^s = -\Re(F_m \bar{u}_m^s) \quad (22)$$

are the rates of exchange of kinetic energy between the two fluids due to mutual friction ( $M_m^n$  being the flow of energy from the normal fluid to the superfluid and  $M_m^s$  the flow from the superfluid to the normal fluid) and

$$\epsilon_{inj}^j = f^n \delta_{m,m'} \Re(u_m^j) \quad (23)$$

are the rate of influx of energy due to the forcing terms, where  $\Re$  and  $\Im$  denote real and imaginary parts respectively. The nonlinear triadic interaction  $T_m^j$  is defined such that the energy flux at shell  $m^*$  is given by

$$\Pi_m^j = \sum_{m \leq m^*} T_m^j \quad (24)$$

$$= \Delta_{n+1}^j - (-b-1)\Delta_n^j, \quad (25)$$

where we define the correlator

$$\Delta_n^j = k_{n-1} \Im(u_{n-1}^j u_n^j u_{n+1}^j), \quad (26)$$

all other terms cancelling due to the conservation of energy.

Fig. 1 (bottom) shows the energy balance in the inertial range. It is apparent that the total energy flux in each shell is zero (solid black diamond). We find that the normal fluid's inertial term (hollow red squares) is balanced by the viscous term (blue hollow triangles), as in ordinary turbulence. On the contrary, the superfluid's inertial term (solid red squares) is balanced by the mutual friction (solid grey circles), in agreement with Roche *et al.* [23]. The inset of Fig. 1 (bottom) shows the energy balance over the entire k-space, including the contribution of the forcing on the shell  $m = 4$ . We observe that  $M_m^n$  and  $M_m^s$  are always of opposite signs, as expected from their definitions, and, almost without exception,  $M_m^n > 0$  and  $M_m^s < 0$ . Furthermore  $D_m^n < 0$  for all  $m$ .

The basic picture did not change when we reduced the temperature to  $T = 1.96$  K (Fig. 2), and then to  $T = 1.44$  K (Fig. 3), again in agreement with experiments [10]. There are however noticeable differences which develop as the temperature is lowered. At high temperature viscous forces provide a sufficient energy sink for both normal fluid and superfluid. As the temperature drops the normal fluid fraction decreases and the superfluid fraction increases. This reduces the ability of the normal fluid viscosity to adequately dissipate the energy. As  $T$  is decreased, both the normal fluid and superfluid spectra extend to the right, towards higher wavenumbers, and the wavenumber,  $k_\ell$ , corresponding to the intervortex spacing, moves progressively to the right. Furthermore at low  $T$  in the normal fluid the viscous dissipation is no longer balanced by the inertial term, but by the mutual friction term (see Fig. 3 bottom).

In their pure states ( $\rho^s = 0$  and  $\rho^n = 0$  respectively) we expect the spectrum of the normal fluid to decay exponentially after  $k_\eta$  (see Eq. 27), the Kolmogorov microscale at which the inertial term is balanced by the viscous dissipation, and the superfluid to continue to cascade like  $k^{-5/3}$ ; a build-up of energy at high  $k$  is thus expected, although the physical interpretation of our model is limited to  $k < k_\ell$ . We can furthermore expect that as we approach these limiting cases the dominant fluid will cause a deviation in the spectrum of the other fluid. L'vov *et al.* [30] derived approximate expressions for each of these cases.

At low temperatures ( $\rho^s \gg \rho^n$ ), the normal fluid spectrum, instead of decaying exponentially for  $k > k_\eta$ , deviates slightly from  $k^{-5/3}$  due to the force exerted on it by the mutual friction. This continues until the length scale, denoted  $k_*$  (see Eq. 28), at which the viscous dissipation balances the mutual friction. Beyond this wavenumber the normal fluid spectrum decays with a power-law  $k^{-17/3}$ ; not exponentially as in the case of classical turbulence. This power-law decay is valid at least until  $k_\ell$ , the wavenumber corresponding to the inter-vortex spacing, at which point the model for the superfluid is no longer valid.

On the other hand, at high temperatures ( $\rho^n \gg \rho^s$ ), the superfluid spectrum beyond  $k_\eta$  is affected by the exponentially decaying normal fluid so that it deviates from its  $k^{-5/3}$  power-law to a steeper slope  $k^{-3}$ . This continues for as long as the mutual friction dominates over the superfluid inertial term. At some wavenumber,  $k_+$  (see Eq. 29), this relationship shifts such that the inertial term becomes dominant and the superfluid spectrum regains the  $k^{-5/3}$  power-law for as long as the model remains valid ( $k < k_\ell$ ).

Following L'vov [30], we define

$$k_\eta = \epsilon^{1/4} \nu^{-3/4}, \quad (27)$$

$$k_\star = \alpha^{1/2} \left( \frac{\rho^s}{\rho^n} \right)^{1/2} Q^{1/4} \nu^{-1/2}, \quad (28)$$

$$k_+ = \alpha^{3/2} Q^{3/4} \epsilon^{-1/2}, \quad (29)$$

where  $\nu = \nu^n$  and  $\epsilon \equiv -dE/dt$  is the mean energy dissipation (per unit mass), which, in the inertial subrange, is approximately constant. In the context of shell models we define

$$\epsilon_m = |u_m|^3 k_m. \quad (30)$$

We furthermore find, due to the efficient locking of the superfluid and normal fluid velocities in the inertial subrange, that  $\epsilon^n \approx \epsilon^s$ , which we refer to as  $\epsilon$  in Eqs. (27,29).

We show the deviation at low temperature in (Fig. 4), in which we show both power-laws and the critical wavenumbers at which the spectra change. We calculate these wavenumbers in accordance with the approximations derived by L'vov *et al.* [30]. The deviations at high temperature are best realised by considering a system of turbulent superfluid  $^3\text{He-B}$  (see below).

As mentioned above, we expect that at a sufficiently low temperature the superfluid energy spectrum builds up at high  $k$ . This is because the only energy sink for the superfluid is the mutual friction which depends on the presence of the normal fluid to dissipate the superfluid energy. We show the development of the build-up of energy in Fig. 5. We produced Fig. 5 by allowing the fluids to attain fully-developed spectra at high temperature. We then reduced the temperature significantly to a finite, fixed temperature well below our previous low  $T$  and monitored the changes in the superfluid spectrum over time. In order to maintain numerical stability, we fixed the values of  $\rho^s$ ,  $\rho^n$  and  $\nu^n$ . Thus the only temperature-dependent variable was  $\alpha$ , which alone dictates the magnitude of the mutual friction felt by the superfluid. The spectrum is seen to change as progressively more energy moves to higher  $k$ . This phenomenon highlights the necessity for an energy sink at high  $k$  such as the Kelvin wave cascade and phonon emission.

In classical turbulence the Reynolds number,  $Re = UD/\nu$ , is a measure of the ratio of the inertial and viscous terms, where  $U$  and  $D$  are the large scale velocity and length scale

respectively. The inertial range exists as long as  $Re \gg 1$ . In the same spirit we may define a quantum Reynolds number as the ratio of the inertial and general dissipative terms, be they due to viscous dissipation or mutual friction. Using this definition we may say that the Reynolds number for the superfluid is temperature-dependent, in agreement with [23]: both normal fluid and superfluid spectra extend to higher wavenumbers as the temperature is decreased.

We furthermore show the dependence of the vortex line density,  $L$ , on the Reynolds number. According to Kolmogorov, the ratio of the dissipation scale and the scale of the large eddies is  $\delta/D \propto Re^{-3/4}$ . In superfluid turbulence the smallest scale is  $\ell \propto L^{-1/2}$ , hence we expect  $L \propto Re^{3/2}$ . We show that this scaling holds true by considering  $Re$  and  $L$  and allowing the forcing to vary between  $f = (1+i) \cdot 5 \cdot 10^{-6}$  and  $f = (1+i) \cdot 5 \cdot 10^1$  in multiples of 10 (see Fig. 6). This finding agrees with the truncated DNS model of Salort *et al.* [31].

## B. Decaying turbulence

To study the decay of turbulence we let  $f = 0$  and start from saturated spectra as an initial condition. We observe that during the decay both the superfluid and normal fluid spectra maintain their initial shape ( $k^{-5/3}$  at low to intermediate values of  $k$ , followed by a more rapid drop at larger  $k$ ), as shown in Fig. 7 (top and bottom). The spectra shown in these figures are the result of ensemble averaging over 10 realisations. We also found that the total turbulent kinetic energy,  $E(t)$ , where

$$E^j(t) = \sum_m \frac{1}{2} |u_m^j(t)|^2, \quad (j = n, s), \quad (31)$$

and the vortex line density,  $L(t)$ , decay as  $E(t) \propto t^{-2}$  and  $L(t) \propto t^{-3/2}$  as shown in Figs 8 and 9, which is in agreement with experiments [32–34] and theoretical models [35].

## C. Forced turbulence in superfluid $^3\text{He-B}$

The other non-radioactive isotope of liquid helium is  $^3\text{He}$ .  $^3\text{He}$  atoms are fermions, having only a single neutron in their nuclei, and achieve superfluidity by the Cooper pairing of two atoms. Although  $T_c$  for  $^4\text{He}$  is about 2.17 K, for  $^3\text{He}$  it is much lower, at about 1 mK.

Experimental studies of  ${}^3\text{He}$  have focused on the so-called B-phase, known as  ${}^3\text{He-B}$ . The most notable physical property of  ${}^3\text{He-B}$  is the rapid increase in the normal fluid viscosity below  $T_c$ , which is proportional to  $1/T^2$  [36]. In fact the viscosity is so great that for all intents and purposes the normal fluid may be considered to be at rest. We may thus consider such a system to be that of a turbulent superfluid in the presence of a stationary normal fluid. This description is equally applicable to that of high temperature  ${}^4\text{He}$  in the wavenumber subrange  $k \gg k_\eta$ . This correspondence has already been noted by L'vov *et al.* [30]. A second relevant physical property is the change in its quantum of circulation such that  $\kappa = h/2m_3$ , or about 2/3 that of  ${}^4\text{He}$ , where  $m_3$  denotes the mass of a  ${}^3\text{He}$  atom.

In a theoretical paper Vinen [26] showed that in superfluid  ${}^3\text{He-B}$  the positions of the dissipative subrange and the inertial subrange are reversed, such that the dissipation due to the mutual friction occurs at low wavenumbers whereas the inertial subrange obeying the  $k^{-5/3}$  power-law is located at high wavenumbers. His prediction for the wavenumber at which this changeover takes place is in agreement with that of L'vov *et al.* [30, 37]. L'vov *et al.* [37] furthermore predicted that the dissipation should follow a  $k^{-3}$  power-law, the same power law as that of high temperature  ${}^4\text{He}$  in the wavenumber subrange  $k \gg k_\eta$  [30].

In order to model turbulence in  ${}^3\text{He-B}$  we reduced our two-fluids shell model back to a single-fluid model, replacing viscous dissipation with a dissipation due to mutual friction. The shell model equation then becomes

$$\frac{d}{dt}u_m^s = G_m[u^s] - F_m + f^s\delta_{m,m'}, \quad (32)$$

where the mutual friction is now of the form

$$F_m = \alpha\kappa^{3He}Lu_m^s. \quad (33)$$

The temperature dependence of Eq. 32 is controlled by the parameter  $\alpha$  alone. Experience has shown that a mutual friction of this form is extremely efficient at dissipating energy and in order to attain a steady spectrum of the kind described in [26, 30, 37] it is necessary both to reduce  $\alpha$  to  $O(10^{-2})$  (much below  $T_c$  and very close to a pure superfluid state) and to increase the forcing to  $O(10^2)$  (5 orders of magnitude greater than that used for  ${}^4\text{He}$ ). The numerical results show the spectrum initially decreasing like  $k^{-3}$  which subsequently changes to  $k^{-5/3}$ . The changeover wavenumber is in reasonably good agreement with  $k_+$  predicted by L'vov (see Fig. 10). We used the following parameters  $(M, \lambda, m') = (20, 2, 4)$ .

## IV. DISCUSSION

We have developed a two-fluids shell model based on the GOY shell model of classical turbulence. We have shown that, in continually excited turbulence, the mutual friction effectively locks together the normal fluid and superfluid over a wide range of wavenumbers, forming a  $k^{-5/3}$  Kolmogorov spectrum. By reducing the temperature and hence the normal fluid fraction, we have shown that this range's cut-offs are temperature-dependent for both the normal fluid and superfluid. In other words, lowering the temperature leads to longer inertial subranges. This result for the energy spectrum agrees with the experiment of Tabeling [10] and the DNS of Roche *et al.* [23]. The relation which we find between vortex line density and Reynolds number agrees with Salort *et al.* [31]. We have realised the deviations from the  $k^{-5/3}$  spectrum due to the mutual friction predicted by L'vov [30] for  $^4\text{He}$  at low temperature and by Vinen [26] and L'vov [30, 37] for  $^3\text{He-B}$ . In the zero-temperature limit our model develops a build-up of energy at high wavenumbers, highlighting the necessity for an energy sink at high  $k$ , such as the Kelvin wave cascade and phonon emission [38]. Our model shares the common advantage of all shell models: being flexible and computationally inexpensive, it is relatively easy to investigate the decay of turbulence, which would be more difficult with DNS. Our results for the decay of turbulence are in agreement with experiments [32–34] and theoretical models [35]. We anticipate that our two-fluids model can be used to study other aspects of quantum turbulence.

## ACKNOWLEDGEMENTS

One of the authors (CFB) is grateful to F. Toschi for stimulating interest in shell models. We also thank V.S L'vov for his comments. This work was made possible with support from the EPSRC.

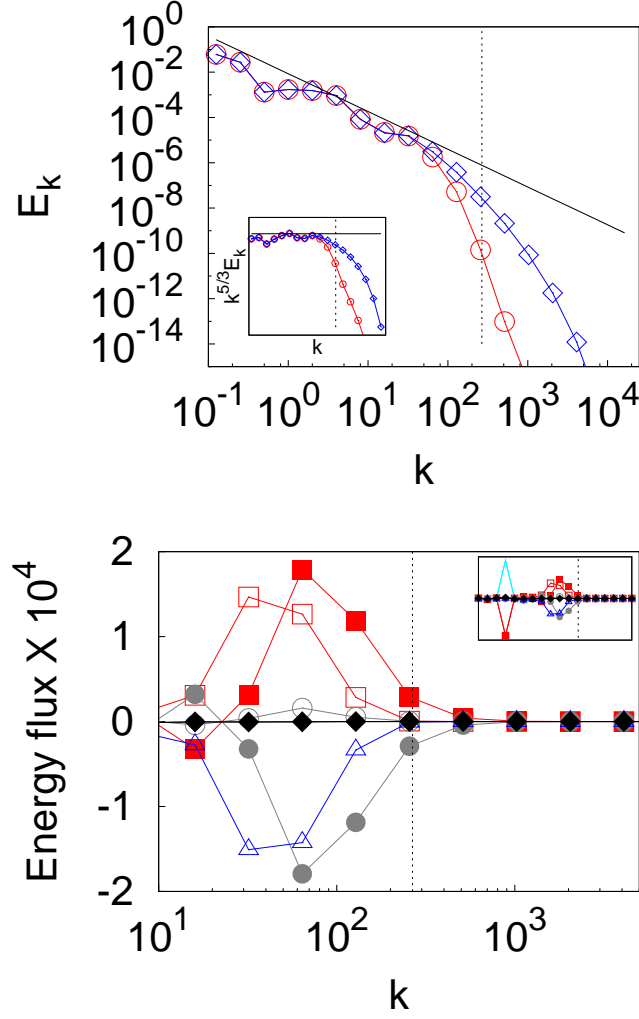


FIG. 1. (Colour online). Top: Main plot: Log-log plot of superfluid (blue diamond) and normal fluid (red circle) energy spectra  $E_k$  ( $\text{cm}^2 \text{s}^{-2}$ ) vs wavenumber  $k$  ( $\text{cm}^{-1}$ ) at  $T = 2.157$  K. The solid line denotes the  $k^{-5/3}$  Kolmogorov spectrum. The vertical dotted line marks  $k_\ell$ . Inset: Compensated spectra. As above, but  $k^{5/3} E_k$  vs  $k$ . Bottom: Main plot: Log-lin plots of time-averaged scale-by-scale energy budget  $dE_k/dt$  ( $\text{cm}^2 \text{s}^{-3}$ ) vs wavenumber  $k$  ( $\text{cm}^{-1}$ ) for the two-fluid model at high temperature (2.157K). We show the fluxes for the normal fluid (hollow shapes) and superfluid (solid shapes). The main plot shows the balance of fluxes in the normal fluid between the inertial term  $T_m^n$  (red squares) and the viscous term  $D_m^n$  (blue triangles), and in the superfluid between the inertial term  $T_m^s$  (red squares) and the mutual friction term  $M_m^s$  (grey circles). We also show the total flux  $dE_m/dt$  (black diamonds). Inset: In the inset we show the fluxes over the entire wavenumber range, including the flux due to the external forcing  $\epsilon_{inj}^{n,s}$  (light blue line) which is nonzero only at shell  $n = 4$ . The vertical dotted line denotes the time-averaged wavenumber,  $k_\ell$ , corresponding to the intervortex spacing.

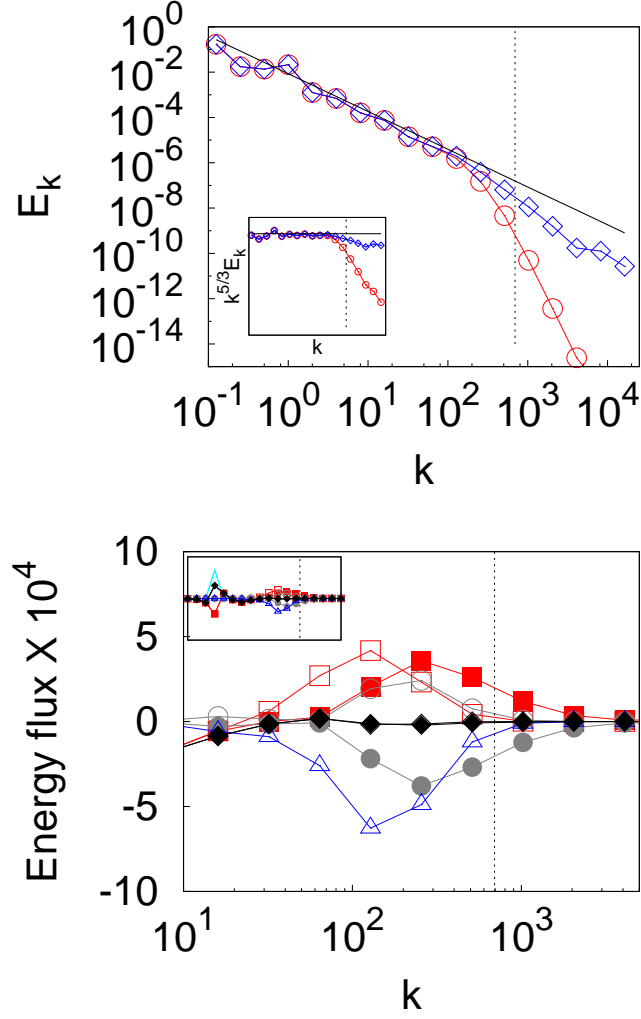


FIG. 2. (Colour online). Top: Main plot: Log-log plot of superfluid (blue diamond) and normal fluid (red circle) energy spectra  $E_k$  ( $\text{cm}^2 \text{s}^{-2}$ ) vs wavenumber  $k$  ( $\text{cm}^{-1}$ ) as in 1 (top) but at  $T = 1.96$  K. The solid line denotes the  $k^{-5/3}$  Kolmogorov spectrum. The vertical dotted line marks  $k_\ell$ . Inset: Compensated spectra. As above, but  $k^{5/3} E_k$  vs  $k$ . Bottom: Main plot: Log-linear plots of time-averaged scale-by-scale energy budget  $dE_k/dt$  ( $\text{cm}^2 \text{s}^{-3}$ ) vs wavenumber  $k$  ( $\text{cm}^{-1}$ ) for the two-fluid model as in 1 (bottom) but at medium temperature (1.96K). We show the fluxes for the normal fluid (hollow shapes) and superfluid (solid shapes). The main plot shows the balance of fluxes in the normal fluid between the inertial term  $T_m^n$  (red squares) and the viscous term  $D_m^n$  (blue triangles), and in the superfluid between the inertial term  $T_m^s$  (red squares) and the mutual friction term  $M_m^s$  (grey circles). We also show the total flux  $dE_m/dt$  (black diamonds). Inset: In the inset we show the fluxes over the entire wavenumber range, including the flux due to the external forcing  $\epsilon_{inj}^{n,s}$  (light blue line) which is nonzero only at shell  $n = 4$ . The vertical dotted line denotes the time-averaged wavenumber,  $k_\ell$ , corresponding to the intervortex spacing.

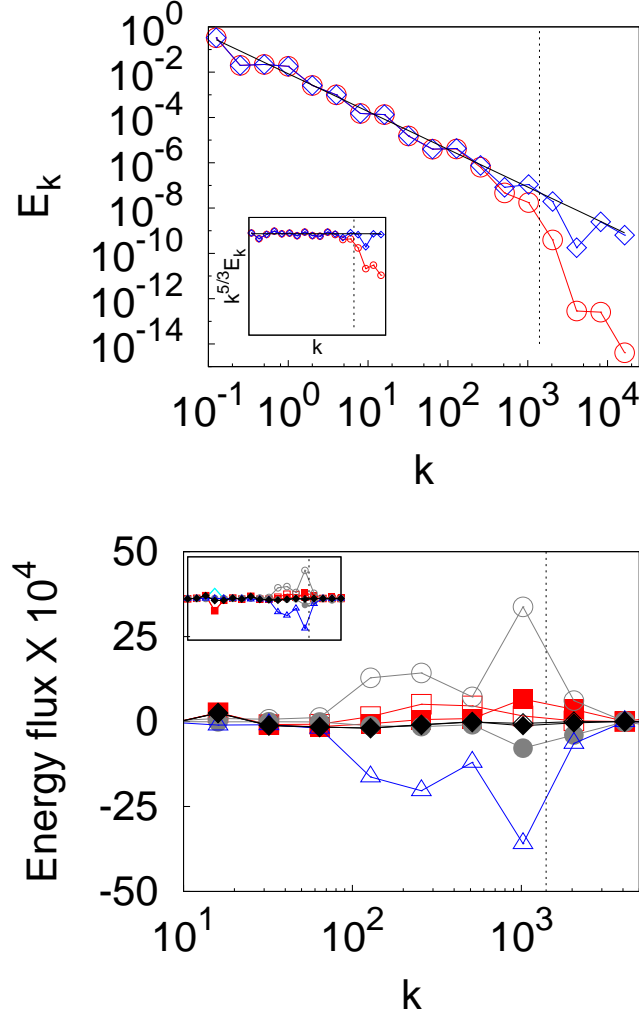


FIG. 3. (Colour online). Top: Main plot: Log-log plot of superfluid (blue diamond) and normal fluid (red circle) energy spectra  $E_k$  ( $\text{cm}^2 \text{s}^{-2}$ ) vs wavenumber  $k$  ( $\text{cm}^{-1}$ ) as in 1 (top) but at  $T = 1.44$  K. The solid line denotes the  $k^{-5/3}$  Kolmogorov spectrum. The vertical dotted line marks  $k_\ell$ . Inset: Compensated spectra. As above, but  $k^{5/3} E_k$  vs  $k$ . Bottom: Main plot: Log-linear plots of time-averaged scale-by-scale energy budget  $dE_k/dt$  ( $\text{cm}^2 \text{s}^{-3}$ ) vs wavenumber  $k$  ( $\text{cm}^{-1}$ ) for the two-fluid model as in 1 (bottom) but at low temperature (1.44K). We show the fluxes for the normal fluid (hollow shapes) and superfluid (solid shapes). The main plot shows the balance of fluxes in the normal fluid between the mutual friction term  $M_m^n$  (red squares) and the viscous term  $D_m^n$  (blue triangles), and in the superfluid between the inertial term  $T_m^s$  (red squares) and the mutual friction term  $M_m^s$  (grey circles). We also show the total flux  $dE_m/dt$  (black diamonds). Inset: In the inset we show the fluxes over the entire wavenumber range, including the flux due to the external forcing  $\epsilon_{inj}^{n,s}$  (light blue line) which is nonzero only at shell  $n = 4$ . The vertical dotted line denotes the time-averaged wavenumber,  $k_\ell$ , corresponding to the intervortex spacing.

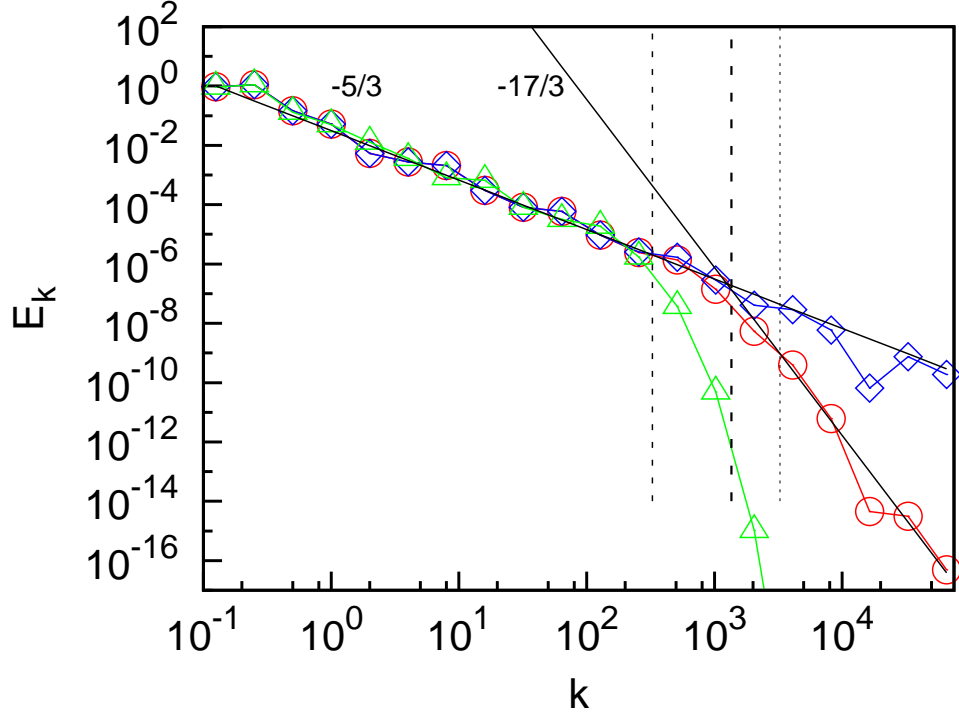


FIG. 4. (Colour online). Log-log plot showing dissipation of turbulent energy in normal fluid at low temperature. Coupled normal fluid (red circles) is seen to deviate from uncoupled normal fluid (green triangles) as a result of mutual friction with superfluid (blue diamonds). Coupled normal fluid follows  $k^{-5/3}$  for  $k < k_\eta$ , deviates slightly for  $k_\eta < k < k_\star$  and follows a  $k^{-17/3}$  power-law for  $k > k_\star$ . The vertical dotted line is  $k_\ell$  and the short- and long-dashed lines are respectively  $k_\eta$  and  $k_\star$ . For clarity  $k_\eta < k_\star < k_\ell$ .

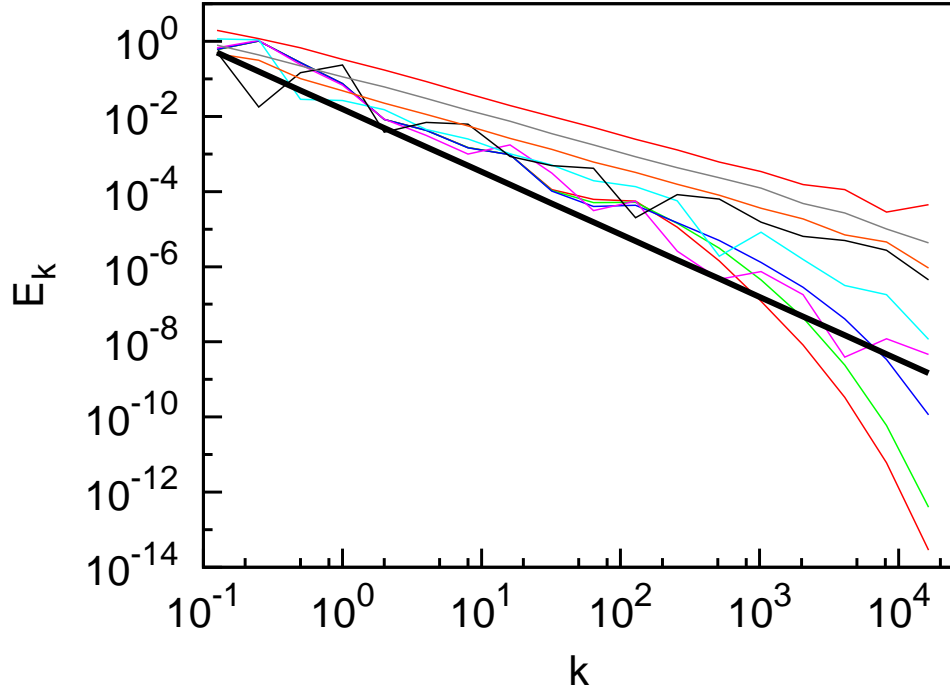


FIG. 5. (Colour online). Log-log plot of development of build-up of energy in superfluid spectrum. Spectra (bottom to top) at time  $t = 0$  (red), 0.025 (green), 0.05 (dark blue), 0.5 (pink), 5 (light blue), 50 (black), 500 (orange), 5000 (grey) and 10000s (red) after lowering the temperature.  $k_l$  (not shown) moves from  $k \approx 10^3$  to  $k \approx 2 \cdot 10^4$  during this period. The thick black line denotes the  $k^{-5/3}$  Kolmogorov spectrum.

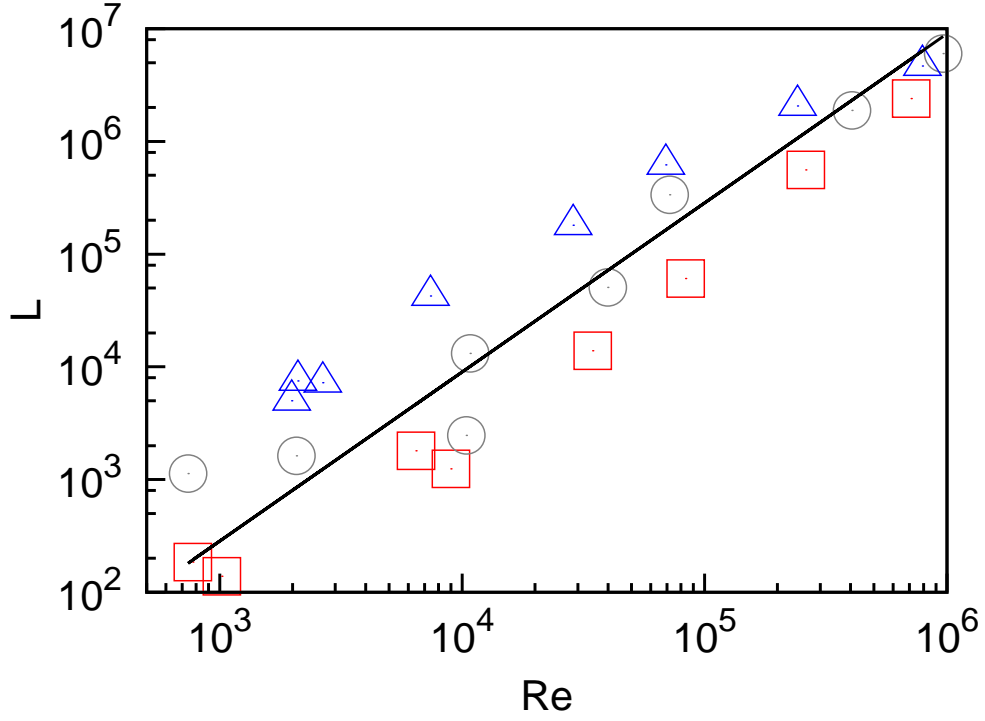


FIG. 6. (Colour online). Log-log plot of vortex line density,  $L$ , vs Reynolds Number,  $Re$ , at all three temperatures: high (red squares), medium (grey circles) and low (blue triangles). The points from left to right correspond to increasing forcing, the leftmost point using forcing  $f = (1 + i) \cdot 5 \cdot 10^{-6}$  and the rightmost point  $f = (1 + i) \cdot 5 \cdot 10^1$ . The Reynolds Number is calculated at the first shell ( $n = 1$ ) giving  $D = 2^4$ . The solid black line is  $L = Re^{3/2}$ .

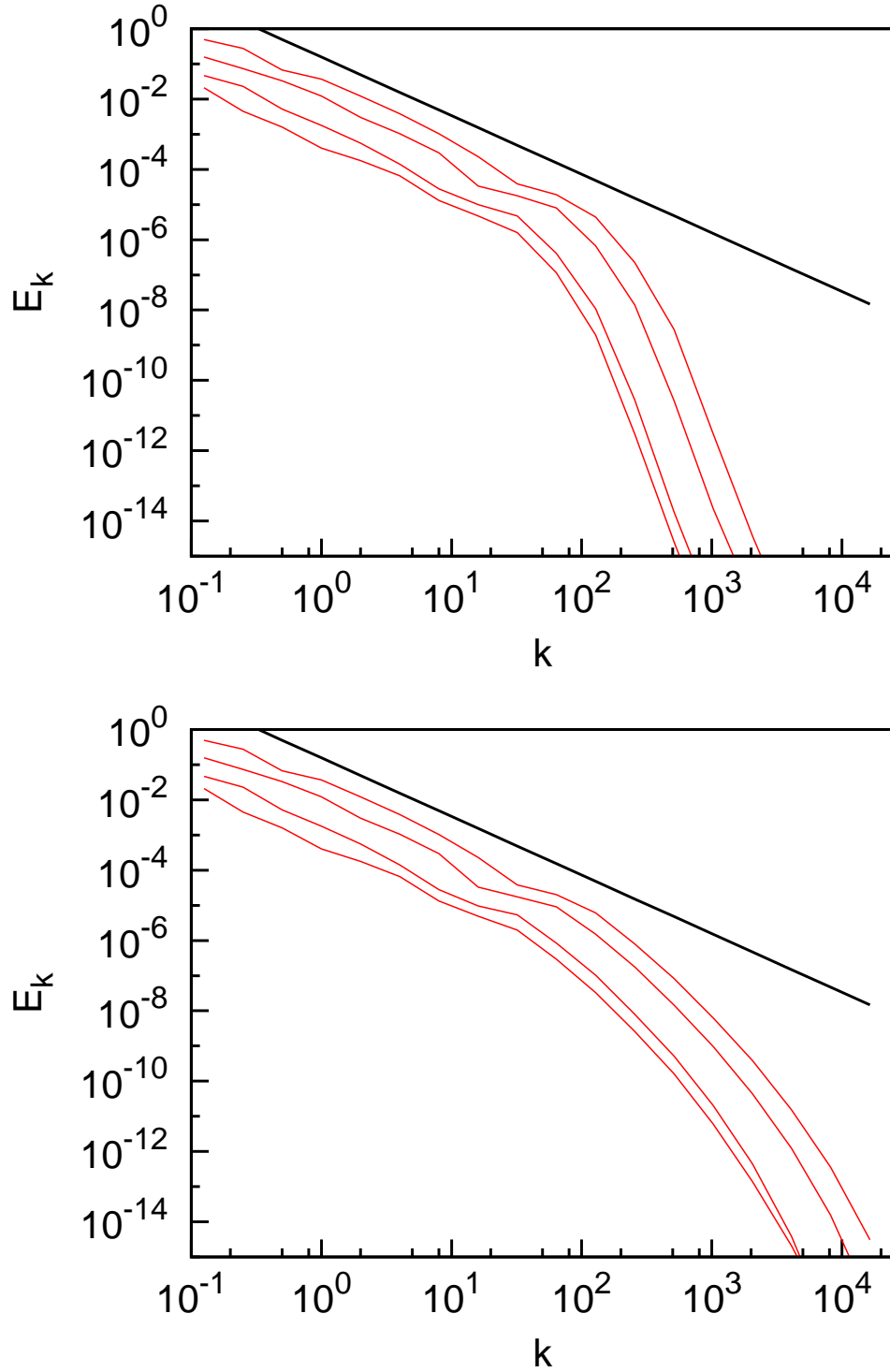


FIG. 7. (Colour online). Decay of energy spectra for normal fluid (top) and superfluid (bottom) over 10 realisations. Spectra top to bottom: After 500, 1000 , 2500 and 5000s. Also shown is the  $k^{-5/3}$  spectrum (solid black line).

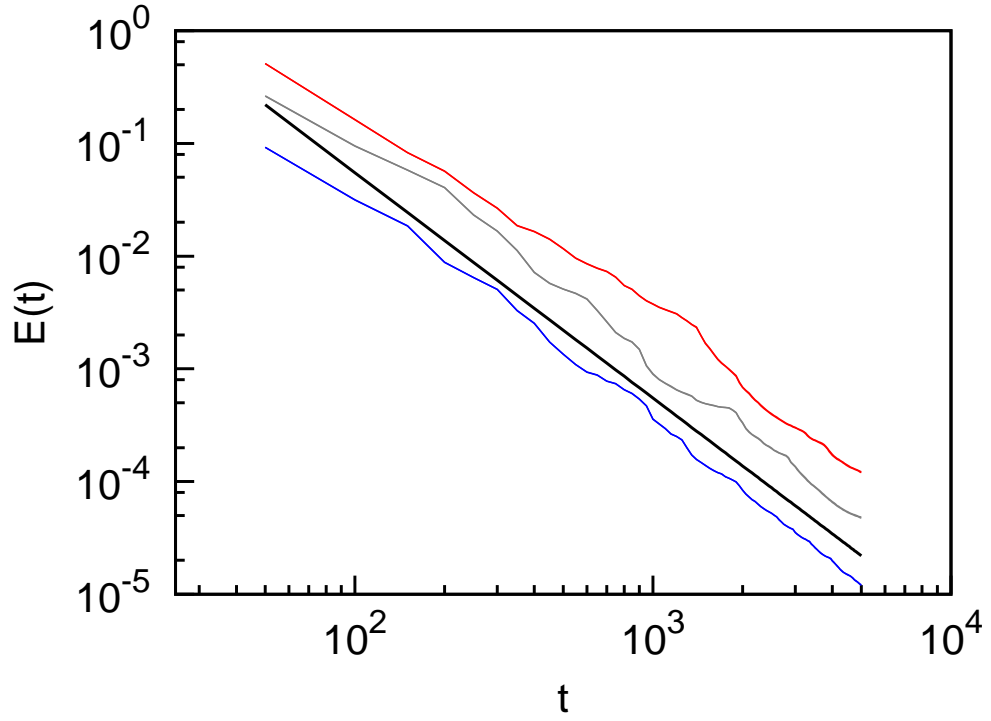


FIG. 8. (Colour online). Decay of total energy over period of 5000s ensemble averaged over 10 realisations. Top to bottom: High (red line), medium (grey line) and low (blue line) temperatures. Shifted to show power law. Also shown is the  $t^{-2}$  spectrum (solid black line).

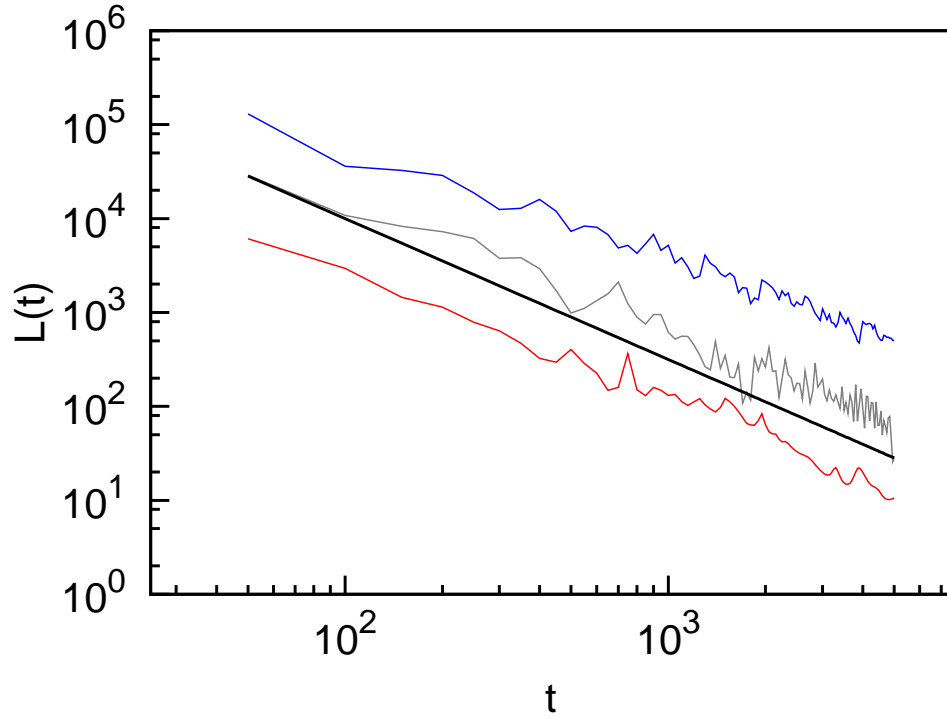


FIG. 9. (Colour online). Decay of vortex line density over period of 5000s ensemble averaged over 10 realisations. Top to bottom: Low (blue line), medium (grey line) and high (red line) temperatures. Data is not shifted. Also shown is the  $t^{-3/2}$  spectrum (solid black line).

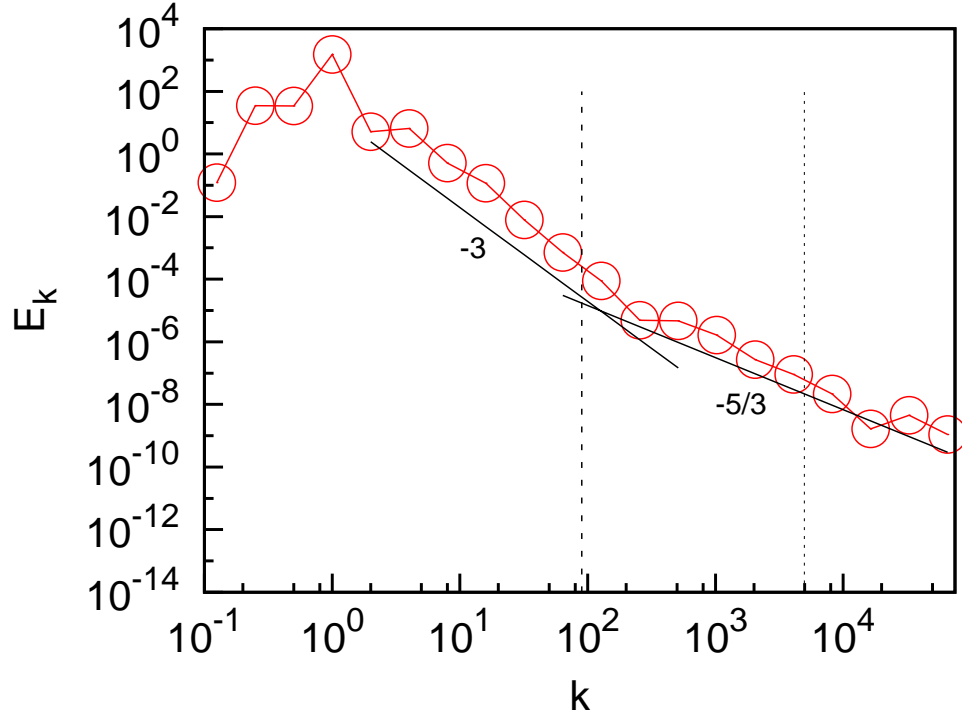


FIG. 10. (Colour online). Log-log plot of fully developed, steady power spectrum for superfluid (red circles) in the presence of a stationary normal fluid in  $^3\text{He-B}$ . We show the two power-laws,  $k^{-3}$  and  $k^{-5/3}$ . The dashed line is  $k_+$ , the wavenumber at which the inertial term becomes of the same order as the mutual friction term, and the dotted line is  $k_\ell$ , the intervortex spacing.

- 
- [1] R.J. Donnelly, *Quantized Vortices In Helium II*, Cambridge University Press, Cambridge, 1991.
- [2] C.F. Barenghi, R.J. Donnelly and W.F. Vinen, *J. Low Temp. Phys.* **52**, 189 (1983).
- [3] M.R. Smith, R.J. Donnelly, N. Goldenfeld and W.F. Vinen, *Phys. Rev. Lett.* **71**, 2583 (1993).
- [4] P.E. Roche, P. Diribarne, T. Didelot, et al. *Europhysics Lett.* **77**, 66002 (2007).
- [5] J. Salort, C. Baudet, B. Castaing, B. Chabaud, F. Daviaud, T. Didelot, P. Diribarne, B. Dubrulle, Y. Gagne, F. Gauthier, A. Girad, B. Hebral, B. Rousset. P. Thibault. and P.-E. Roche, *Phys. of Fluids* **22**, 125102 (2010).
- [6] D. Schmoranzer, M. Kralova, V. Pilcova, W.F. Vinen, and L. Skrbek, *Phys. Rev. E* **81**, 066316 (2010).
- [7] W.F. Vinen and J.J. Niemela, *J. Low Temp. Phys.* **128**, 167 (2002).
- [8] P.L. Walstrom J.G. Weisend, J.R. Maddocks, and S.W. Van Sciver, *Cryogenics* **28**, 101 (1988).
- [9] M.R. Smith, D.K. Hilton, and S.W. Van Sciver, *Phys. of Fluids* **11**, 751 (1999).
- [10] J. Maurer and P. Tabeling, *Europhys. Lett.* **43**, 29 (1998).
- [11] A.W. Baggaley and C.F. Barenghi, *Phys. Rev. B* **84**, 020504 (2011).
- [12] H. Adachi, S. Fujiyama, and M. Tsubota, *Phys. Rev. B* **81**, 104511 (2010).
- [13] K.W. Schwarz, *Phys. Rev. B* **38**, 2398 (1988).
- [14] L. Biferale, *Ann. Rev. Fluid Mechanics* **35**, 441 (2003).
- [15] U. Frisch, *Turbulence: The legacy of A.N. Kolmogorov*, Cambridge University Press, Cambridge, 1995.
- [16] L.Ts. Adzhemyan, M. Hnatich, D. Horvath and M. Stehlik, *Phys. Rev. E* **58**, 4511 (1998).
- [17] E.B. Gledzer, *Phys. Dokl.* **18**, 216 (1973).
- [18] M. Yamada and K. Ohkitani, *J. Phys. Soc. Japan* **56**, 4210 (1987).
- [19] V.S. L'vov, E. Podivilov, A. Pomyalov, I. Procaccia. and D. Vandembroucq, *Phys. Rev. E* **58**, 1811 (1998).
- [20] H.E. Hall and W.F. Vinen, *Proc. Roy. Soc A* **238**, 204 (1956); H.E. Hall and W.F. Vinen, *Proc. Roy. Soc A* **238**, 215 (1956).
- [21] C.F. Barenghi, *Phys. Rev. B* **45**, 2290 (1992).
- [22] C.J. Gorter and J.H. Mellink, *Physica* **15**, 285 (1949).

- [23] P.-E. Roche, C.F. Barenghi and E. Leveque, *Europhys. Lett.* **87**, 54006 (2009).
- [24] J.T. Tough, *Progress in Low Temperature Physics*, vol. 8, ed. D.F. Brewer (1982).
- [25] D.J. Melotte and C.F. Barenghi, *Phys. Rev. Lett.* **80**, 4181 (1998).
- [26] W.F. Vinen, *Phys. Rev. B* **71**, 024513 (2005).
- [27] R.J. Donnelly and C.F. Barenghi, *J. Phys. Chem. Ref. Data* **27**, 1217 (1998).
- [28] L. Merahi, P. Sagant and M. Abidat, *Europhys. Lett.* **75**, 757 (2006).
- [29] C.F. Barenghi, S. Hulton and D.C. Samuels, *Phys. Rev. Lett.* **89**, 275301 (2002).
- [30] V.S. L'vov, S.V. Nazarenko and L. Skrbek, *J. Low Temp. Phys.* **145**, 125 (2006).
- [31] J. Salort, P.-E. Roche, and E. Leveque, *Europhys. Lett.* **94**, 24001 (2011).
- [32] S.R. Stalp, L. Skrbek and R.J. Donnelly *Phys. Rev. Lett.* **82**, 4831 (1999).
- [33] P.M. Walmsley, A.I. Golov, H.E. Hall, A.A. Levchenko and W.F. Vinen *Phys. Rev. Lett.* **99**, 265302 (2007).
- [34] P.M. Walmsley, A.I. Golov, H.E. Hall, W.F. Vinen and A.A. Levchenko *J. Low Temp. Phys.* **153**, 127 (2008).
- [35] L. Skrbek, J.J. Niemela and R.J. Donnelly, *Phys. Rev. Lett.* **85**, 2973 (2000).
- [36] L.D. Landau and E.M. Lifshitz, *Fluid Mechanics*, Pergamon Press, New York, 1987.
- [37] V.S. L'vov, S.V. Nazarenko and G.E. Volovik *JETP Lett.* **80**, 535 (2004).
- [38] A.W. Baggaley and C.F. Barenghi, *Phys. Rev. B* **83**, 134509 (2011).